ERDC/CHL CHETN-IX-65
August 2023

US Army Corps of Engineers®

Sensitivity of Simulated Flaw-Height Estimates to Phased Array Scan Parameters

By Jason D. Ray, James S. Kinnebrew, Ramsay D. Bell, and Martin T. Schultz

PURPOSE: Phased array ultrasonic testing (PAUT) is a nondestructive testing (NDT) technique for detecting and sizing flaws in welds. Estimates of flaw size are sensitive to a variety of PAUT scan parameters. In this study, estimates of flaw height are simulated using computer software. The sensitivity of these estimates to selected PAUT scan parameters is analyzed to identify those that have the greatest influence on estimates of flaw height. Understanding how varying different parameters within a phased array instrument affects the accuracy of flaw-height estimates helps to validate PAUT scan procedures and improve flaw-height estimates. For this research, a series of permutations on selected flaws were performed to see how certain parameters affect the accuracy in sizing flaw height. In addition, an analysis on how beam spread leads to flaw sizing inaccuracies was also conducted as part of this work.

BACKGROUND: Discontinuities are interruptions of the typical structure of a material, such as a lack of homogeneity in its mechanical, metallurgical, or physical characteristics. Discontinuities that exist within the welds of an in-service hydraulic steel structure (HSS) may reduce its ability to perform as intended and to increase risks to life and property. Discontinuities can be introduced either as an artifact of manufacture or as damage accumulated over time as the result of the repetitive stress and strain caused by routine use of the structure. When performing fitness-for-service analysis, it is important to detect and size discontinuities in structural members of the HSS so that the need for repair of the structure can be evaluated. Because many of these discontinuities may be hidden within the welds of in-service HSS, NDT methods are needed to detect and size them.

While NDT and PAUT have been used for many years in the oil and gas industry and numerous other industries, the unique geometries and weld configurations encountered in HSS make the applications of PAUT to these structures more challenging. The work described in this technical note is motivated by the need to develop and test NDT procedures that are specifically aimed at detecting and sizing flaws in HSS. Steel specimens representing geometries and weld configurations commonly encountered in HSS were manufactured to contain discontinuities embedded in known locations within the welds. American Society of Non-destructive Testing (ASNT) Level III–certified technicians were contracted to develop NDT procedures for flaw detection and sizing in these specimens using PAUT.

This technical note describes an effort to simulate the NDT procedures proposed for these specimens using specialized computer software and to estimate the height of the discontinuities embedded in the steel specimens from simulation results. CIVA by EXTENDE was chosen as the modeling software to accomplish this task (EXTENDE, n.d.). CIVA simulates multiple inspections methods: ultrasonic testing (UT), PAUT, eddy current testing, radiographic testing, computed tomography, and guided-wave testing, offering advanced beam, inspection, and analysis tools all within the standard UT module. EXTENDE is the only authorized distributor of CIVA in the United States.

As-built drawings of the specimens were used as the basis for constructing 3D computer-aided design (i.e., CAD) models to represent the steel specimens. Most discontinuities were represented in two dimensions regardless of whether or not the actual flaw type was planar, volumetric, or laminar, except when the flaw was an inclusion. The sensitivity of height estimates to variation of selected PAUT scan parameters was investigated by varying these parameters in a one-at-a-time fashion and recalculating height. The objective of sensitivity analysis was to determine whether the error in height estimates might be reduced by adjusting the proposed PAUT scan parameters proposed by the ASNT Level III technicians.

Flaws can be detected and sized in a wide variety of different materials using NDT methods. Conventional UT, which uses high-frequency sound waves to locate and size flaws, was introduced more than 50 yr ago.[*] With conventional UT, flaws are located and sized by scanning welds using a transducer that contains single or dual piezoelectric crystals. The PAUT transducer contains many piezoelectric crystals that pulse at different time intervals to help the technician focus the sound beam and, with the aid of a computer, visualize more complex shapes.

There are a variety of different ways to estimate the height of a flaw based on how the ultrasonic energy interacts with the flaw. Examples of these techniques include amplitude, multiple wave mode, and time-based (such as tip diffraction) (Schmerr et al. 2013; Birring 2010).

Amplitude or decibel-drop sizing is a technique where the size of the discontinuity or flaw is proportional to the amplitude of the reflected signal. Birring describes two fundamental flaws with this method that prevent it from being little more than a qualitative method of determining if a flaw is present or not: (1) if the flaw is larger than the beam spread, then there is no change in the amplitude of the reflected signal, and (2) the reflected signal does not change proportionately with discontinuity size (Birring 2010). In practice, this is also known as the decibel-drop method and is one of the most widely used techniques. The start and stop locations of a flaw along any axis are associated with those locations where the amplitude of the sound reflecting off the flaw decreases by a certain amplitude, typically −3, −6, or −12 dB. The decibel-drop method works best when the flaw is larger than the beam spread. If the beam spread is larger than the flaw, the decibel drop will reflect the limits of the beam spread rather than the limits of the flaw. The decibel-drop method is applied to phased array with the difference being that phased array attempts to eliminate the need for measuring and multiple offsets from the weld by scanning multiple angles from a single position instead of being limited to what the sensor and wedge allows.

Multiple wave-mode flaw sizing is a technique where the different wave modes of the ultrasonic signal are used. Specifically, the longitudinal and the shear wave component's arrival time from reflecting off the flaw provides the estimation. These waves, when reflected off surfaces, can mode convert into the other type of wave (i.e., a longitudinal wave that reflects off of a flaw creates reflections that contain a longitudinal and a shear-wave component.)

---

[*] For a full list of the spelled-out forms of the units of measure and unit conversions used in this document, please refer to *US Government Publishing Office Style Manual*, 31st ed. (Washington, DC: US Government Publishing Office 2016), 248–52 and 345–7, respectively. *https://www.govinfo.gov/content/pkg/GPO-STYLEMANUAL-2016/pdf/GPO-STYLEMANUAL-2016.pdf*.

Tip diffraction utilizes diffraction off of the tips of well-defined internal cracks and defects. Crack-tip diffraction can be performed using a single probe in a style called *pulse-echo* where the same probe is used to both send and receive the acoustic energy and *pitch-catch* where two probes on opposite sides of the weld are used where one transmits the acoustic energy and the other receives it. The pitch-catch version of crack-tip diffraction is known as time-of-flight diffraction; however, both of these methods use the time-of-flight of the ultrasonic signals off of the tips of the flaws to size.

PAUT can be utilized to perform any of the aforementioned sizing techniques. PAUT utilizes an array of piezoelectric crystals to steer the beam over an array of angles. By firing the crystals of the array in specific patterns, typically set by the instrument, PAUT is capable of scanning a large cross section of the specimen from a single location. Coupled with techniques such as the decibel-drop method, flaw sizing can be performed in less time with less complexity.

The advantages and disadvantages of the various techniques described above are summarized in Table 1.

Table 1. Flaw-sizing technique comparison.

Technique	Advantages	Disadvantages
Amplitude/Decibel Drop	• Easy in concept but difficult in accurate execution • Useful for quick assessments • Widely used • Required by many codes and recommended procedures	• Basic idea of discontinuity size • Dependent on flaw orientation • Accurate sizing requires flaws that are larger than the beam width • Thicker specimens are more prone to beam width related sizing anomalies
Multiple-Wave Mode	• Used to evaluate a flaw as a percentage of wall thickness • Used to find internal diameter and outside diameter cracks	• Difficult to distinguish signals in welds due to mode conversion. Velocity of modes differ and cannot be distinguished with most instruments • Higher level of training required
Diffraction/Time Techniques	• Works well on surface-connected reflectors • Becoming integrated into codes • Most accurate • Fast • Good for thick materials • Permanent record • Excellent probability of detection	• Tip diffracted signal are weak in amplitude • Tip signal can be mistaken by other earlier arriving signals • Requires more training than other methods • Dead zone at scanning surface and backwall reflection boundary • Not suitable for thinner materials (less than 0.50 in.) • Not good for complex geometries • Dedicated time of flight diffraction (TOFD) probes are more expensive • TOFD requires multiple probes

For this study, flaw height is the difference between the top and bottom edge of the flaw. Therefore, the accuracy of a flaw-height estimate will depend on the ability to accurately locate the start and stop locations of the flaw. The ability to locate start and stop locations in a particular weld can depend upon the types of probes used and their settings as well as geometry and weld configurations.

METHOD: PAUT scan procedures were simulated over 10 flaws in seven steel specimens. Flaw size was estimated using the decibel-drop method with an attenuation of −6 dB as the cutoff. The sensitivity of flaw-size estimates was assessed with respect to four scan parameters: frequency, incident dimension, number of elements, and element width. Frequency defines the frequency of the excitation signal injected into the specimen. Frequency affects the resolution of the reflector: the higher the frequency, the better the resolution but also the more attenuation. Incident dimension is the size of the active aperture of the probe, which is the number of phase-array elements multiplied by the element size. The number of elements describes how many piezoelectric crystals are contained in the probe. The element width is the width of the piezoelectric crystals.

Ideally, PAUT scans should be conducted from all accessible specimen faces and angles to minimize the amount of error in detecting flaws and estimating flaw height. However, long simulation run times necessitated scanning each specimen from one side only. Therefore, PAUT scans were conducted from the side that provided the best chance of hitting the flaw perpendicularly in the first leg of the sound path, prior to hitting the back wall of the specimen. The second leg of the sound path is that which follows an interaction between the sound path and the flaw or backwall of the specimen. The second leg of the sound path was usually ignored. However, some specimen geometries and flaw locations did not allow for this, and the second leg of the sound path was used.

The several PAUT scan parameters that were varied in sensitivity analysis and their respective levels are summarized in Table 2. For each parameter variation, the amount increased and decreased from the median value is 25% except for frequency, which included two more commonly used frequencies, 7.5 MHz and 10 MHz.

Table 2. Phased-array probe permutation parameters.

Permutation	Frequency (MHz)	Incident Dimension (mm)	Number of Elements	Element Width (mm)
1 (Nominal)	5	31.92	32	0.92
2	3.75	31.92	32	0.92
3	6.25	31.92	32	0.92
4	7.5	31.92	32	0.92
5	10	31.92	32	0.92
6	5	25.536	32	0.72
7	5	39.9	32	1.6928
8	5	23.92	24	0.92
9	5	39.92	40	0.92
10	5	31.92	32	0.736
11	5	39.28	32	1.15

The nominal permutation represents a commonly used transducer in the industry made by the Olympus Corporation, Weld Series 5L32-A32 (Olympus, n.d.), with the accompanying wedge, SA32-N55S. The values highlighted in *blue* are the values that were changed with each permutation. CIVA automatically adjusts parameters to account for the chosen parameter's values. For example, in Permutation 6, the Incident Dimension was set to 25.536 mm, 25% less than the nominal value of 31.92 mm, and CIVA automatically adjusts the Element Width parameter to 0.72 mm with the nominal value being 0.92 mm.

CIVA settings used to simulate PAUT scans are summarized in Table 3. Other software settings were left at their default values for a PAUT model.

Table 3. CIVA settings.

CIVA Setting	Value
Phased Array Crystal Settings	
Pattern	Linear Phased Array
*Incident Dimension	31.92 mm
Elevation	10 mm
*Number of Elements	32
Gap Between Elements	0.08 mm
*Element Width	0.92 mm
—	
Wedge Settings	
Wedge Geometry	Flat
Wedge Front Length	28.006 mm
Wedge Back Length	33.494 mm
Wedge Width	40 mm
Wedge Height	25.099 mm
Crystal Refraction Angle	54.764°
Crystal Incidence Angle	36.1°
Squint Angle	0°
Disorientation	0°
Wave Type	Transverse
Longitudinal Wave Velocity	5900 m/s
Transverse Wave Velocity	3230 m/s
Signal Settings	
Signal Choice	Hanning
*Center Frequency	5 MHz
Bandwidth	50% at −6 dB
Phase	0°
Number of Points	512

CIVA Setting	Value
Phased Array Scan Settings	
Focusing Type	Sectorial Scanning
**Initial Angle	50°
**Final Angle	72°
**Number of Steps	44
Step Size	0.5°
Reference Frame	Along normal
Wave Type	Transversal Waves
Amplitude Law	Uniform
Model Computation Settings	
Computation Mode	3D
Field / Reflector Interaction	Full Incident Beam
Field Accuracy	1
Defect Accuracy	1
Account for Attenuation	No
Active Mode Identification	Yes
Number of Modes to Return	5
***Sound Path	Direct
Line Scan Settings	
Scan Step	0.5 mm/deg
**Number of Steps	25
Increment Skip	Raster

*These are settings that are altered depending on the model that is running. Shown are the nominal values from Table 2.
**These settings are changed depending on the specimen and flaw location.
***When possible, only the first leg of the sound path is considered; however, some flaws required the second leg.

The decibel-drop method is demonstrated here using a hypothetical flaw to avoid revealing flaw locations in the actual specimens. The actual specimens exhibit a variety of geometries. Each specimen contains multiple flaws exhibiting a wide variety of characteristics such as type, length, height, aspect ratio, location, and tilt. The flaw characteristics with regards to the specimens they exist in are intentionally not described in this technical note to preserve the ability to use these specimens in future blind testing.

Each specimen was scanned using a 5L32-A32 probe and an SA32-N55S wedge made by Olympus. The computation was set such that only reflections on the flaw from direct hits in the first leg were accounted for. The wedge was placed such that the full height of the flaw is encompassed within the sector scan; this resulted in shot angles ranging from 50° to 72° with a 0.5° resolution, resulting in up to 44 angle steps for the scan, as illustrated in Figure 1*a*. The figure also shows the specimen rotated 90° to the weld. The scan path of the probe is shown along with a visual indication of where the flaw is, Figure 1*b*. The scan path bounds are set by trial and error to minimize computation time and obtain the limits of the flaw return. For this example, a scan path of (25) 0.5 mm steps was chosen.

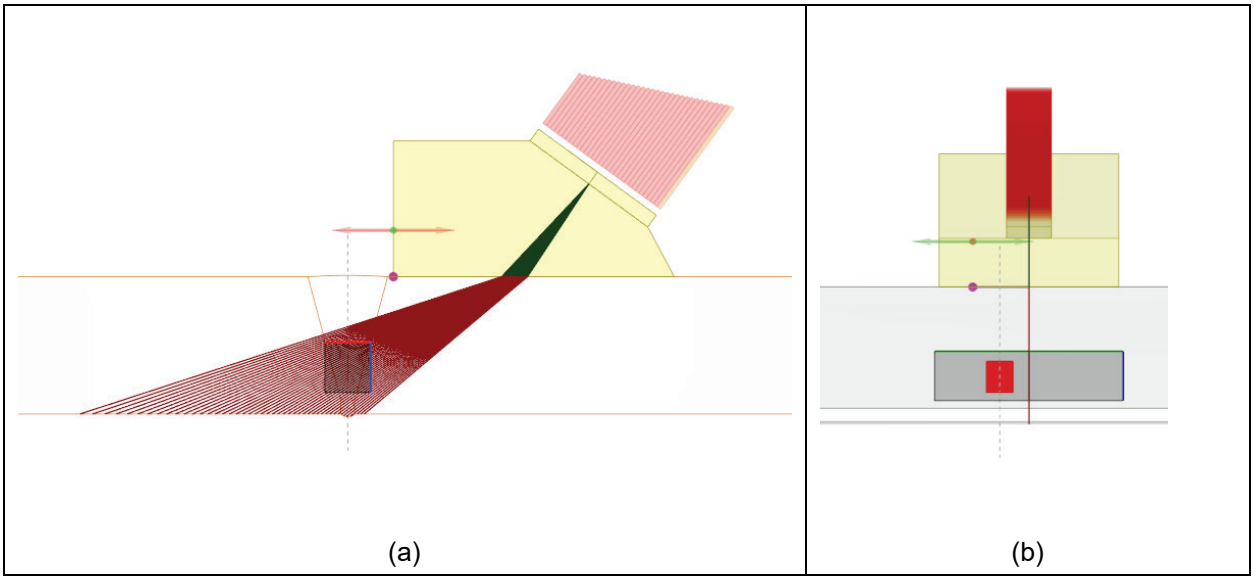

Figure 1. Example flaw: (*a*) view perpendicular to the scan path illustrating the different shots of the sector scan; (*b*) view from behind the probe and parallel to the scan path demonstrating how the probe is used to measure flaw length.

For the purposes of this study, two main visualizations of the data are used: the *C*-scan and the *S*-scan. To understand what these visualization techniques are, an understanding of the *A*-scan is necessary. *A*-scans provide time-series information of how the ultrasonic signal propagates in the specimen. The amplitude of the signal describes the signal reflection, and the time instance translates to distance from the probe. The *C*-scan and *S*-scan are two methods of representing the collected *A*-scans from the different angles and positions along the weld. By aggregating the *A*-scan results from the line scan, extracting the peak amplitude, and plotting the amplitudes onto an *X*-*Y* plot, the *C*-scan is obtained. For the results represented from CIVA, the *x*-axis is the shot number or the angle that was tested. The *y*-axis is the testing position along the weld. Peak amplitudes at each point on this plot create a heat map that can be used to assist in flaw sizing. The *C*-scan does not contain depth information, so the height of the flaw cannot be determined using

this method, though the length and width can. Similar to the *C*-scan, the *S*-scan is a heat map of data but provides different information. The *x*-axis is the *A*-scan of that specific shot, and the *y*-axis is depth. Only a single step along the weld is shown at a time, but the single step is used for flaw-height sizing. Visual representations of these two visualization methods are shown in Figure 2 through Figure 6. These figures contain cursors that are used for sizing.

Starting with Figure 2, a flaw and scan represented as a *C*-scan, the two cursors on the plot are set to the peak amplitude obtained in comparison to every index and shot performed on the scan. The *C*-scan color gradient shades the peak scan of the collection in a very *light blue*. The length of the flaw is determined by setting the cursors to the first index positions along the *y*-axis that meet the criteria of being at least −6 dB from the peak. The difference between the two cursors results in the flaw length, in increments of 0.5 mm as that was the resolution used (Figure 3).

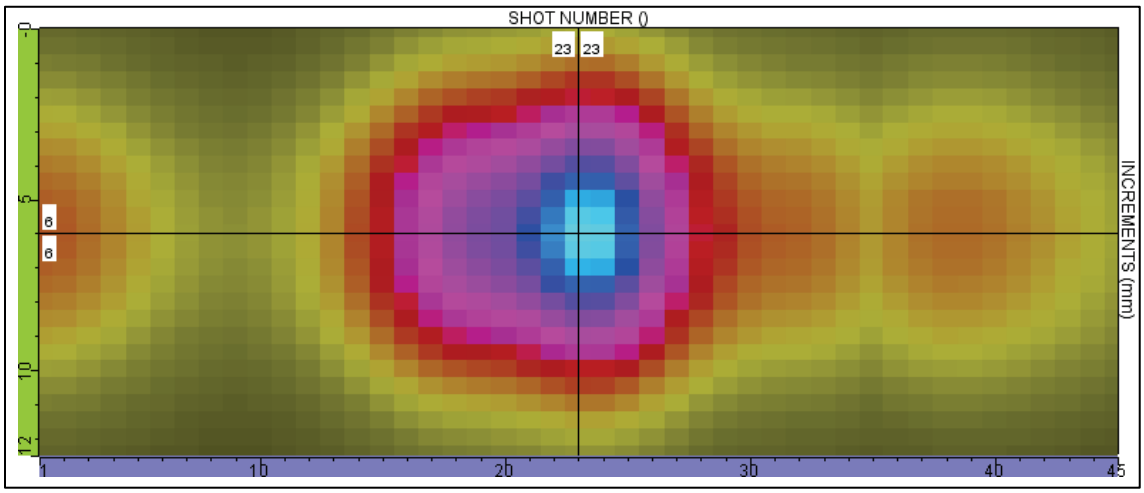

Figure 2. *C*-scan starting cursor position; maximum amplitude of the scan.

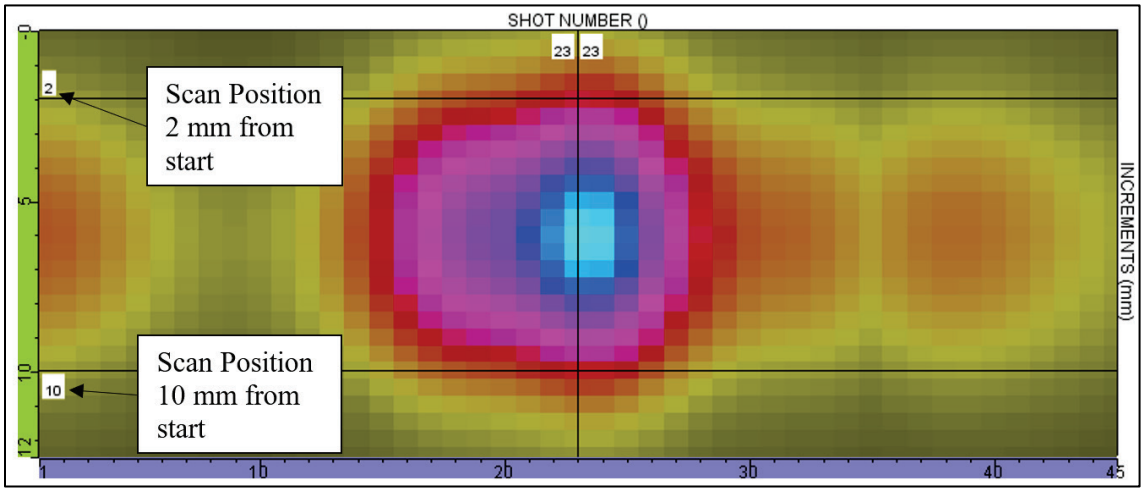

Figure 3. *C*-scan −6 dB point on the index axis; length limits.

The *C*-scan can be used to set bounds along the shot axis in a similar manner (Figure 4).

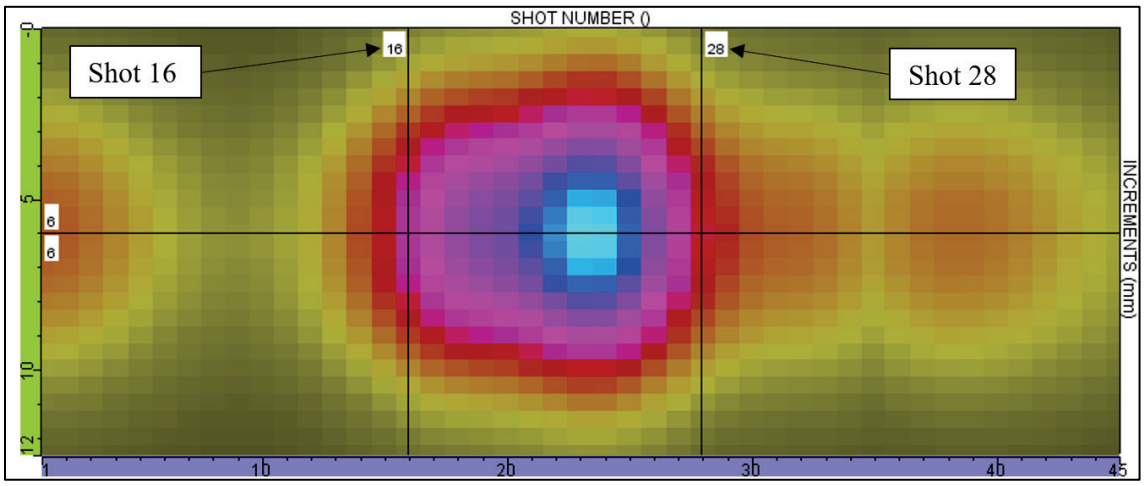

Figure 4. *C*-scan −6 dB point on the shot axis; used to set position on *S*-scan.

The cursors for shot number are the angles of the phased array sector scan that hit at least −6 dB. This, however, does not directly give height. There can be other high-amplitude reflections unrelated to the flaw or from a different leg of the shot. To extrapolate flaw height, the amount of time it takes for that peak to be hit along with the angle is considered in the *S*-scan. Setting the cursors on along the sound path or *A*-scan of the angles within the *S*-scan allows a line from one cursor to the other to be drawn, which gives flaw height (Figure 5 and Figure 6).

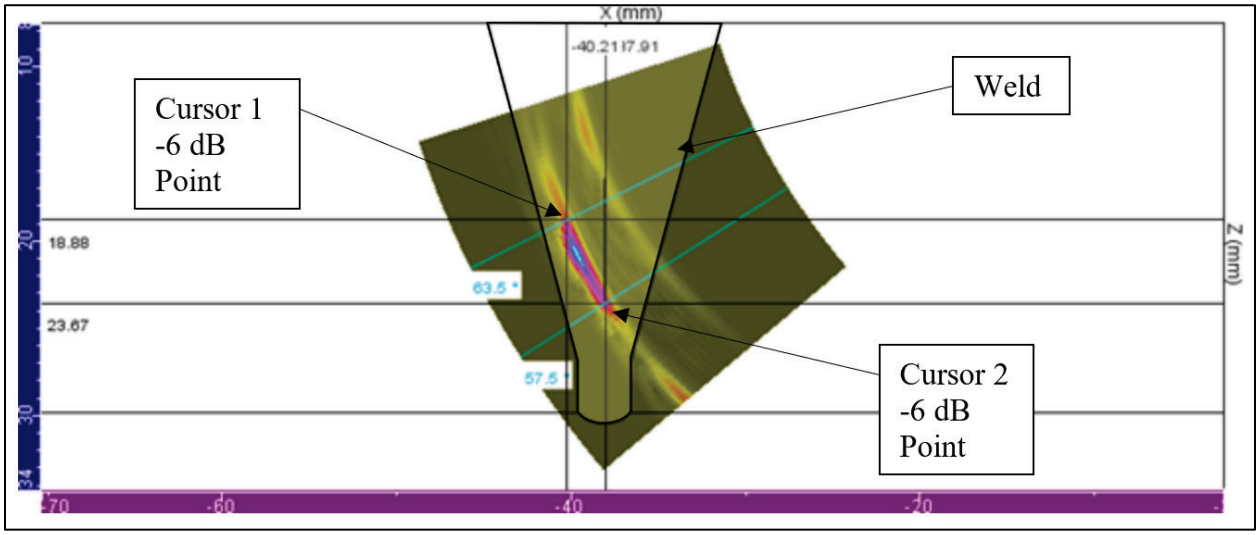

Figure 5. Using the *S*-scan for flaw-height sizing.

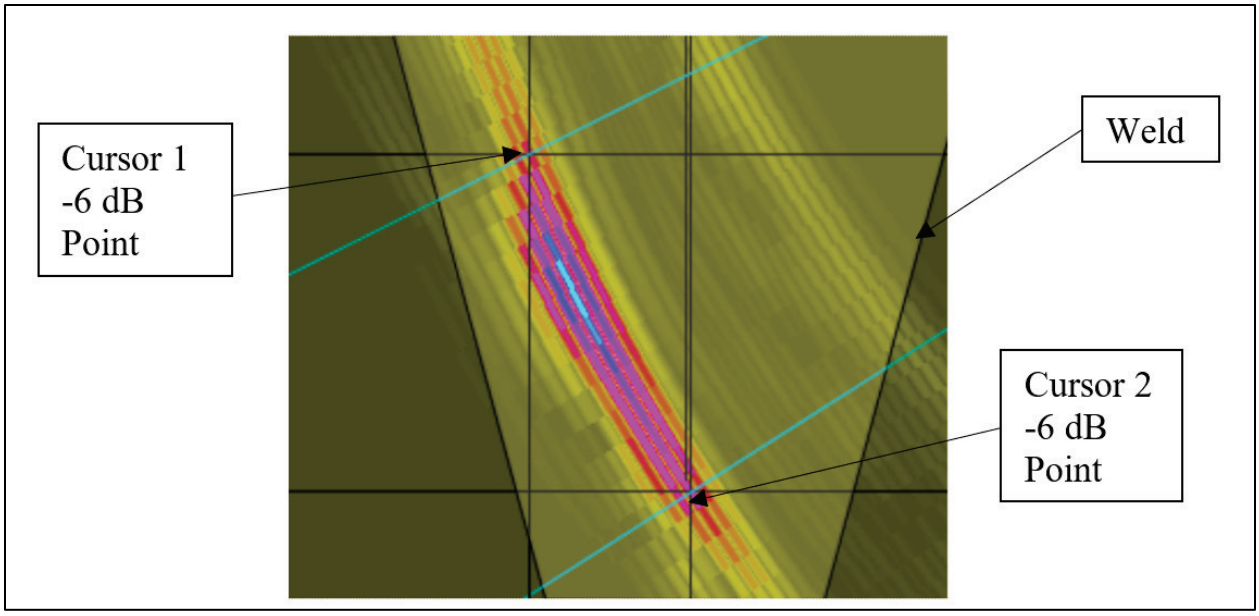

Figure 6. *S*-scan zoomed in.

CIVA provides a measurement toolbar where these values are tracked (Figure 7). Two height values are displayed here, ΔV and D, where ΔV is the distance between the two horizontal portions of the cursors and D is the distance from one cursor crosshair to the other. D is the value used in this study as there are flaws that are tilted.

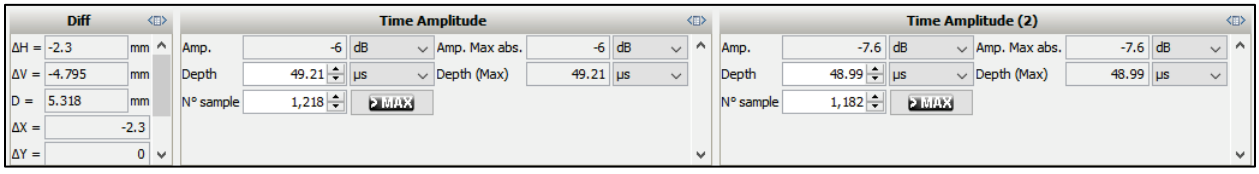

Figure 7. Cursor positioning and flaw height.

For this example, the probe dimensions are the nominal case from Table 2. Using the tools within CIVA by placing the cursors, the measured flaw height for this example is 5.318 mm with the actual height being 6 mm. The results are that the flaw was undersized by 0.682 mm.

This method of sizing for flaw height was performed on each of the 10 flaws chosen and 11 permutations of the probe parameters. The 10 flaws and their dimensions that the experiments were performed on are described in Table 4.

RESULTS: For the 11 permutations listed in Table 2, the same model run was performed encompassing a line scan from a single index offset along the weld. At this time, the actual details of the flaws cannot be revealed. Instead, the differences between the known flaw height and the calculated dimensions were compared based upon the method detailed in Figure 2 through Figure 7. Percent error in flaw-height estimates is listed in Table 5. Positive values of percent error indicate flaw height was overestimated, and a negative value indicates flaw height was underestimated.

Table 4. Flaw information.

#	Flaw and Weld Type	Flaw Height (mm)	Flaw Length (mm)
1	Lack of Fusion in Single Vee	2.032	14.478
2	Lack of Fusion in Double Vee (subsurface)	2.449	6.096
3	Lack of Fusion in Double Vee (subsurface)	8.636	32.258
4	Cylindrical Inclusion in Single Vee (weld groove area)	2.54	177.292
5	Lack of Fusion in Double Vee (sub-surface)	6.35	11
6	Lack of Fusion in Single Vee (base metal)	*36.068	36.068
7	Lack of Fusion in Single Vee	5.842	13.97
8	Cylindrical Inclusion in Single Vee (weld groove area)	5.334	14.224
9	Lack of Fusion in Single Vee	9.144	19.304
10	Lack of Fusion in Single Vee	5.08	7.112

*The reported height is the width of the lamination. The procedure used to estimate lamination width is the same as that used to estimate flaw height.

Table 5. Percent error in flaw-height estimates.

#	Parameter	Value	Flaw 1	Flaw 2	Flaw 3	Flaw 4	Flaw 5	Flaw 6*	Flaw 7	Flaw 8	Flaw 9	Flaw 10
1	Nominal/Base Case	Nominal	−34.5%	185.7%	−89.7%	196.9%	33.5%	−71.5%	14.8%	45.9%	−33.6%	2.4%
2	Frequency	3.75	−34.6%	166.6%	−86.9%	123.2%	17.4%	−79.7%	−10.7%	45.8%	−41.3%	15.4%
3	Frequency	6.25	−47.3%	166.1%	−91.5%	196.9%	35.0%	−67.4%	57.9%	45.9%	−26.2%	−25.8%
4	Frequency	7.5	−60.7%	145.1%	−92.8%	196.6%	41.0%	−67.4%	96.1%	24.4%	−26.1%	−25.8%
5	Frequency	10	−73.7%	104.3%	−94.2%	196.4%	−29.4%	−81.5%	90.2%	−4.3%	−33.2%	−40.3%
6	Incident Dimension	25.536	−32.1%	104.3%	−86.9%	196.9%	6.9%	−83.8%	−21.6%	−5.3%	−48.3%	16.1%
7	Incident Dimension	39.9	−51.2%	200.0%	−91.5%	196.9%	94.1%	−60.9%	10.9%	36.2%	−15.6%	−11.6%
8	Number of Elements	24	−19.5%	84.4%	−86.7%	196.9%	6.9%	−83.8%	−21.1%	−23.4%	−40.9%	2.3%
9	Number of Elements	40	−48.7%	192.0%	−93.6%	196.6%	92.5%	−58.5%	20.9%	34.5%	−14.9%	−17.3%
10	Element Width	0.736	−34.4%	104.3%	−86.6%	196.9%	6.9%	−81.7%	−27.8%	−5.3%	−41.1%	37.0%
11	Element Width	1.15	−50.9%	186.2%	−94.2%	178.0%	88.4%	−60.0%	30.5%	33.5%	−11.8%	−11.6%

*The reported values are errors in flaw width rather than height. The procedure used to estimate lamination width is the same as that used to estimate flaw height.

Starting with Flaw 1, this model had the probe placed in a position such that the flaw's face was perpendicular to the scan index offset with the central angle in the range of 50° to 72° in the middle of the flaw. The flaw was angled due to being lack of fusion in single vee and followed the angle of the weld vee. For the nominal case, the upper portion of the flaw within the *S*-scan extends beyond the 72° of the scan range. Permutation 8 reduced the undersizing from −34.5% to −19.5%. In terms of millimeters, this increased the measured height from 1.329 mm to 1.636 mm. As the upper portion of the flaw was outside of the scan range, it cannot be determined if the flaw was truly undersized or if it would have been oversized considering how small the flaw is.

Flaw 2 showed oversizing on a flaw where the probe was positioned such that the first leg was perpendicular to the face of the flaw. Unlike Flaw 1, the scan range was able to encompass the entirety of the flaw from the single index point. The height of this flaw was the second smallest within the group. Based upon the results, it appears that the accuracy of the measurement is less oversized as the active aperture decreases.

Flaw 3 was similar to Flaw 2 except the acoustic energy focused on the bottom tip of the flaw, which makes the flaw appear greatly undersized. This could be in part due to the angle of the flaw within the specimen in relation to where the probe was positioned. The first leg hit was not directly perpendicular as it was not possible to be and still scan the flaw within the 50° to 72° range. Changing parameter values had little effect on the results.

Flaw 4 was modeled as cylindrical inclusion whereas the other flaws, except Flaw 8, were modeled as lack of fusion. The *S*-scan results required more in-depth analysis due to strong reflectors off the top and bottom of the cylinders. Most of the energy was centered on the edge of the inclusion closest to the scan face; however, the −6 dB points extended far beyond the bounds of the scan range in every case.

Flaw 5 results exhibit the least sensitivity to adjusting the parameters. The flaw height is among the largest, and the location of the probe in relation to the flaw allows for capturing a quality reflector. Permutations 6, 8, and 10 reduce the size of the active aperture, which in turn reduces oversizing of the flaw.

Flaw 6 height and length are equal, but the measured results for the height are largely undersized. This is due in part to how the probe was positioned to adhere to the scan range defined. Based upon the results, it shows the inverse of Flaw 5. In this case, increasing the active aperture increased the flaw sizing results that were undersized.

Flaw 7 orientation in relation to the face the probe was on was parallel. This led to difficulty in interpreting results. However, due to knowledge of where the flaw was, it was possible to size the acoustic signatures using the *C*-scan and *S*-scan results. For this flaw, the nominal case was relatively accurate with respect to the other permutations. The trend follows that when the active aperture decreased, the flaw is more undersized, and when the active aperture is increased, the flaw is more oversized.

Flaw 8 was modeled as cylindrical inclusion like Flaw 4. For this flaw, increasing the frequency to 7 and 10 MHz reduced oversizing much to the same effect as reducing the active aperture size. Based on the equations presented in the discussion, frequency should have a similar effect to accuracy as

the active aperture size. This was not seen to this degree in the other flaws, but frequency does still have an effect across the collection.

Flaw 9 is perpendicular to the scan face but not perpendicular to the sound path. It is also touching the opposite face with one tip of the flaw. These results start undersized, but as the active aperture size is increased, the accuracy of the height estimation increases.

Flaw 10 is very similar to Flaw 9 in both location and scan position. However, the flaw is almost half the height. The nominal permutation and adjusting the number of elements to 24 gave the most accurate results while decreasing the element width resulted in the most oversized result, and 10 MHz resulted in the most undersized.

All four observed parameters are used in the calculation for beam spread as the incident dimension is encompassed by the element width and the number of elements. For five of the flaws tested, the parameter that minimized error was adjusting the number of elements in the probe. For instance, in Flaws 1, 2, 5, and 10, the error was minimized by adjusting the number of elements from 32 to 24. For Flaw 6, it was minimized by increasing the number of elements to 40.

DISCUSSION: To understand the effects of beam spread, the following discussion provides an overview of how the different parameters effect the size of the beam. In addition, three of parameterization results are analyzed within CIVA's beam tool to show how the beam size changes with different parameter values.

Birring states that the active aperture size and frequency plays the largest roll in whether a flaw is accurately sized or not, depending on the thickness of the material (Birring 2021). He suggests using a 5 MHz probe with an active aperture of at least 0.64 × the part thickness as a general rule. Three of the four parameters tested directly affect the size of the active aperture, and the fourth is varying the frequency. In all cases where parameters related to the active aperture are varied, the excitation frequency is held constant at 5 MHz.

One cause of error comes from how the beam spreads as it propagates throughout the specimen as well as how centralized the acoustic energy is. Beam spread is mathematically described by the following equation that encompasses dimensions of the probe, wedge, and specimen using a round monocrystal probe (Ciorau et al. 2011).

$$\Phi_{eff-6\,dB} = \frac{1.4 \cdot V_{tw} \cdot SPD_{(wedge+specimen)}}{f \cdot D_{eff\,probe}},$$

where

$\Phi_{eff-6\,dB}$ = beam diameter for pulse-echo (mm),
V_{tw} = sheer wave velocity (mm/μs),
$SPD_{(wedge+specimen)}$ = total sound path in the wedge and specimen (mm),
f = nominal frequency (MHz or μs^{-1}), and
$D_{eff\,probe}$ = probe effective diameter (mm).

$$D_{eff\ probe} = D_{probe} \cdot \frac{\cos\beta}{\cos\alpha},$$

where

D_{probe} = probe actual diameter (mm),
β = refracted angle, and
α = wedge angle.

When applied to a one-dimensional array of phased array elements, a similar formulation is used to estimate the beam spread at a specific distance along the sound path that included the wedge (Olympus 2005). Two measurements are considered, the beam length, $\Delta Y_{-6\,dB}$, and the beam width, $\Delta X_{-6\,dB}$.

$$\Delta Y_{-6\,dB} = \frac{0.884 \cdot SPD_{(wedge+specimen)} \cdot V_{specimen}}{f \cdot W_{passive}},$$

$$\Delta X_{-6\,dB} = \frac{0.884 \cdot SPD_{(wedge+specimen)} \cdot V_{specimen}}{f \cdot A_{active} \cos\beta},$$

where

$V_{specimen}$ = ultrasound velocity in specimen (mm/μs),
$W_{passive}$ = length of passive aperture (mm), and
A_{active} = length of active aperture (mm).

$$A_{active} = n \cdot e + g \cdot (n - 1),$$

where

n = number of elements,
e = element width (mm), and
g = gap between two adjacent elements (mm).

By using a combination of these two equations, Olympus says that beam length, $\Delta Y_{-6\,dB}$, estimations are used in part for flaw length measurements while beam width, $\Delta X_{-6\,dB}$, is used in part for flaw height measurements. Note that these formulas were originally developed based upon testing defects such as side-drilled holes and flat-bottomed holes and are accurate within 15%–30%.

CIVA was used to model the beam spread within three specimens representing three extreme cases for flaw height from the study: most oversized, Flaw 2, Permutation 7 (Figure 8); most undersized, Flaw 3, Permutation 5 (Figure 9); and most accurate, Flaw 10, Permutation 8 (Figure 10). Here, a volumetric slice of the beam at the location of the flaw at a single index point along the weld is modeled with the results shown along the *Y*-*Z*-, *X*-*Y*-, and *X*-*Z*-axes. For Figure 8 and Figure 9, the

beam spread in the *Y-Z*-axis is the direction flaw height, and length would be measured. For Figure 10, the *X-Y* axis is used. On each plot, a bounding back is drawn around where the −6 dB point of the beam spread lies along with the dimensions of the beam spread shown in *white*.

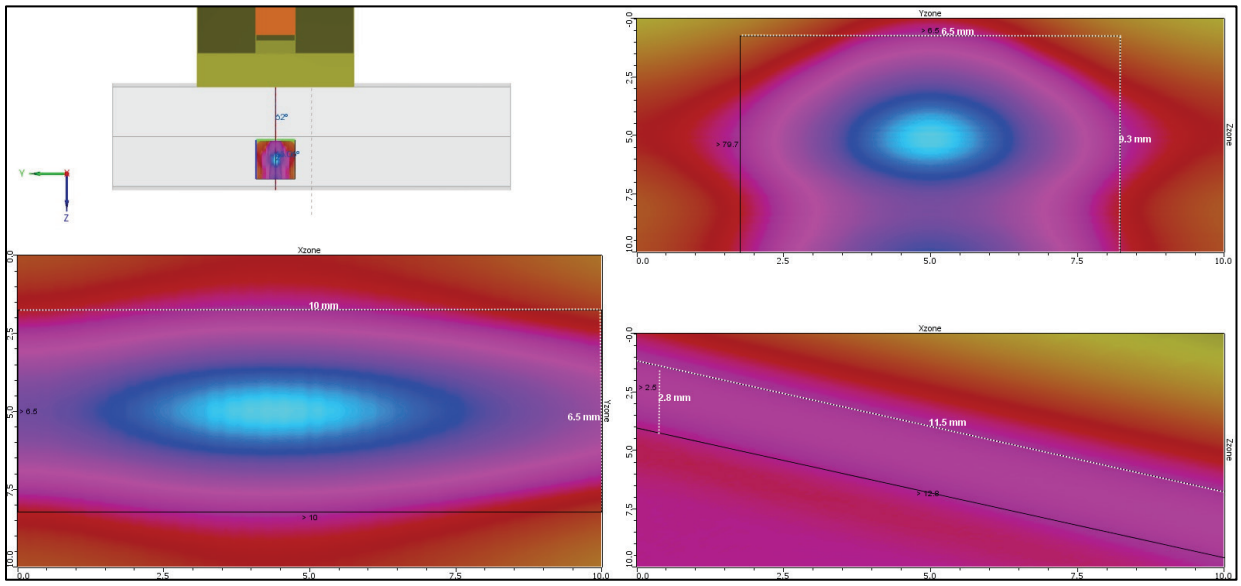

Figure 8. Flaw 2; Permutation 7 beam spread.

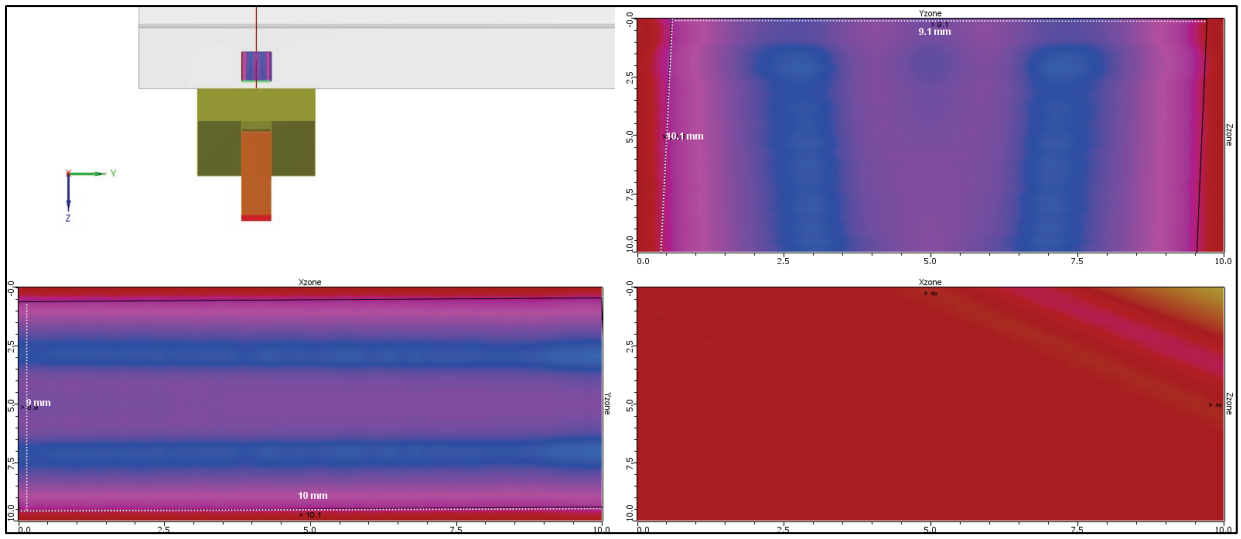

Figure 9. Flaw 3; Permutation 5 beam spread.

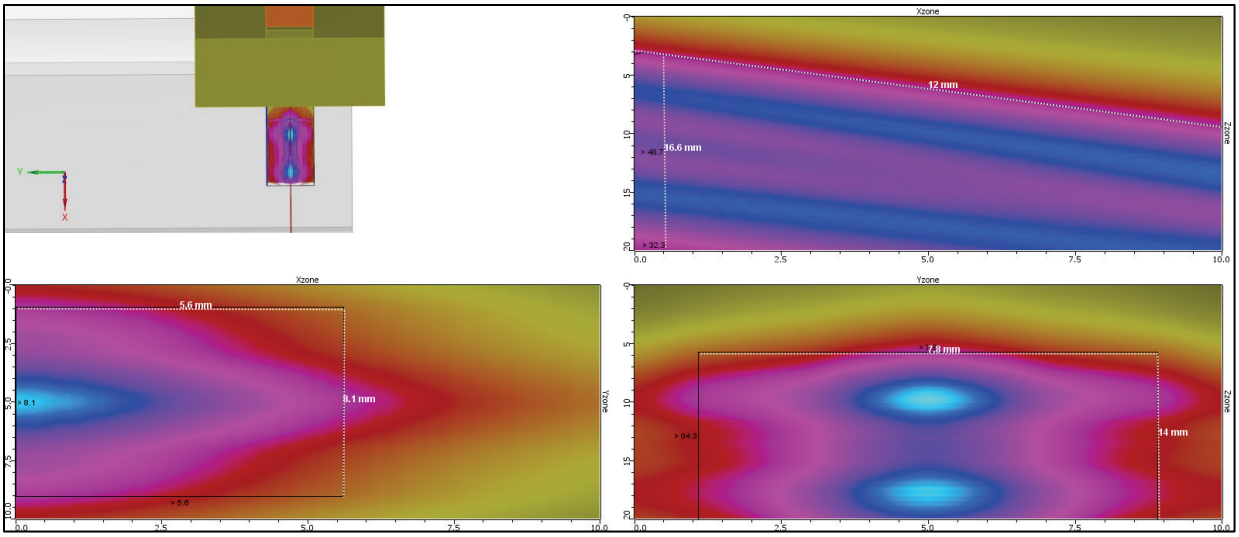

Figure 10. Flaw 10; Permutation 8 beam spread.

Table 6 compiles the results of the three, three-beam spread analyses. The table lists the actual length and height of each flaw, the percentage error in length and height estimates, and the height and length of the beam spread. The beam spread was always greater than the height of each flaw. For Flaw 3, the original flaw sizing was undersized by −94.2%, which shows that beam spread is not the only cause of inaccurate flaws. In this particular scenario, the flaw was tilted toward the probe at 12°, so a straight hit was not possible; it could have been a candidate for a second leg hit.

Table 6. Flaw compared to beam spread.

Flaw	Height Percentage Error	Flaw Height (mm)	Beam Spread Height (mm)	Length Percentage Error	Flaw Length (mm)	Beam Spread Length (mm)
2*	200.0%	2.449	9.8	31.2%	6.096	6.5
3**	−94.2%	8.636	10.1 (cuts off)	0.8%	32.258	9.1
10***	2.3%	5.08	8.1	19.5%	7.112	5.6

* 21° tilt away from the probe
** 12° tilt toward the probe
*** 90° with respect to the specimen

On the contrary, flaw length better demonstrates how beam spread affects sizing accuracy. Looking at Flaw 2, the known flaw length is 6.096 mm, and the beam spread −6 dB boundary for that dimension is 6.5 mm. This means the beam spread is larger than the flaw, which resulted in a 31.2% oversizing. For Flaw 10, the flaw is also oversized even though the beam spread is less than the flaw length. For Flaw 3, the beam spread, 9.1 mm, is much less than the flaw length, 32.258 mm, and the error in the estimate of flaw length is 0.8%.

To provide a better understanding of how beam spread could lead to inaccurate results, a visual example of how the beam interacts with flaws is provided in Figure 11.

Figure 11. A 2 MHz excitation signal (*top*) compared to 10 MHz excitation signal (*bottom*) generated in CIVA.

For these two trials, this example uses the same model parameters for the probe, wedge, flaw, and positioning. The flaw is placed at a depth that is halfway through the specimen angled at 45° to match the refraction angle of the sound path and provide a surface to return the most energy to the transducer. What is illustrated in this example is how the 2 MHz excitation signal envelopes the flaw with some energy passing over the boundary edge while the 10 MHz signal is more concentrated on the flaw with the beam not even encompassing the full flaw. This further illustrates why rastering, the process of physically moving the probe and testing along multiple points, both perpendicular and parallel to the weld, is necessary to accurately size.

SUMMARY: This research investigates the effect of PAUT probe settings on the error in estimates of flaw height. CIVA, a commercial software package, was used to simulate PAUT scans to estimate the height of 10 different flaws in seven different weld specimens. Using CIVA, 11 permutations encompassing four parameters that define how the transducer was modeled and flaw-height sizing was performed on the different permutations. In most cases, it appears that beam spread and focusing most greatly affects how accurate results can be. All four observed parameters are used in the calculation for beam spread as the incident dimension is encompassed by the element width and the number of elements. For five of the flaws tested, the parameter that minimized error was adjusting the number of elements in the probe.

ADDITIONAL INFORMATION: This Coastal and Hydraulics Engineering technical note was prepared by Mr. Jason Ray and Mr. James Kinnebrew, US Army Engineer Research and Development Center (ERDC), Information Technology Laboratory; Mr. Ramsay Bell, US Army Corps of Engineers, Portland District; and Dr. Martin Schultz, ERDC Environmental Laboratory. The research was supported by the ERDC Navigation Systems Research Program under the leadership of Ms. Morgan Johnston. This report should be cited as follows:

> Ray, Jason D., James S. Kinnebrew, Ramsay D. Bell, and Martin T. Schultz. 2023. *Sensitivity of Simulated Flaw-Size Heights to Phased Array Scan Parameters.* ERDC/CHL CHETN-IX-65. Vicksburg, MS: US Army Engineer Research and Development Center. http://dx.doi.org/10.21079/11681/47403.

REFERENCES

Birring, Anmol. 2010. "Sizing Discontinuities by Ultrasonics." *Materials Evaluation* 68:1208–1215.

Birring, Anmol. 2021. "Optimizing Probe Active Aperture for Phased Array Weld Inspections." *Materials Evaluation* 79 (8): 797–801.

Ciorau, Peter, Jason Coulas, and Tim Armitt. 2011. "A Contribution to Length Sizing of Weld Flaws Using Conventional, PAUT and TOFD Ultrasonic Techniques." *e-Journal of Nondestructive Testing* 16(11). https://www.ndt.net/search/docs.php3?id=11174.

EXTENDE. n.d. *EXTENDE CIVA.* Accessed 21 March 2022. https://www.extende.com/available-civa-version.

Olympus. 2005. *Introduction to Phased Array Ultrasonic Technology Applications.* Waltham: Olympus. https://www.olympus-ims.com/en/books/pa/pa-intro/.

Olympus. n.d. Accessed 17 March 2022. https://www.olympus-ims.com/en/probes/pa/weld-series/.

Schmerr, Lester W., Brady J. Engle, Alexander Sedov, and Xiongbing Li. 2013. "Ultrasonic Flaw Sizing–An Overview." *American Institute of Physics* 1511 (1): 1817–1824.